Acta Cryst. (1998). B**54**, 18–28

Investigation into the Crystal Structure of the Perovskite Lead Hafnate, $PbHfO_3$

D. L. CORKER,[a]* A. M. GLAZER,[a] W. KAMINSKY,[a] R. W. WHATMORE,[b] J. DEC[c] AND K. ROLEDER[c]

[a]*Department of Physics, Clarendon Laboratory, Parks Road, The University of Oxford, Oxford OX1 3PU, England,* [b]*School of Industrial and Manufacturing Science, Cranfield University, Cranfield, Bedfordshire MK43 OAL, England, and* [c]*Institute of Physics, Silesian University, Uniwersytecka 4, 40-007 Katowice, Poland.*
E-mail: d.corker1@physics.oxford.ac.uk

(*Received 26 February 1997; accepted 19 June 1997*)

Abstract

The room-temperature crystal structure of the perovskite lead hafnate $PbHfO_3$ is investigated using both low-temperature single crystal X-ray diffraction (Mo $K\alpha$ radiation, λ = 0.71069 Å) and polycrystalline neutron diffraction (D1A instrument, ILL, λ = 1.90788 Å). Single crystal X-ray data at 100 K: space group *Pbam*, a = 5.856 (1), b = 11.729 (3), c = 8.212 (2) Å, V = 564.04 Å^3 with Z = 8, μ = 97.2 mm^{-1}, $F(000)$ = 1424, final R = 0.038, wR = 0.045 over 439 reflections with $F > 1.4\sigma(F)$. Polycrystalline neutron data at 383 K: a = 5.8582 (3), b = 11.7224 (5), c = 8.2246 (3) Å, V = 564.80 Å^3 with χ^2 = 1.62. Although lead hafnate has been thought to be isostructural with lead zirconate, no complete structure determination has been reported, as crystal structure analysis in both these materials is not straightforward. One of the main difficulties encountered is the determination of the oxygen positions, as necessary information lies in extremely weak $l = 2n + 1$ X-ray reflections. To maximize the intensity of these reflections the X-ray data are collected at 100 K with unusually long scans, a procedure which had previously been found successful with lead zirconate. In order to establish that no phase transitions exist between room temperature and 100 K, and hence that the collected X-ray data are relevant to the room-temperature structure, birefringence measurements for both $PbZrO_3$ and $PbHfO_3$ are also reported.

1. Introduction

Structural studies of lead hafnate, $PbHfO_3$, have to date been very limited, including only simple symmetry investigations (Dernier & Remeika, 1975), analysis by polycrystalline X-ray diffraction (Zaitsev *et al.*, 1979) and high-temperature induced phase transitions (Shirane & Pepinsky, 1953; Leont'ev *et al.*, 1984). Although the structure has always been assumed to be isostructural with lead zirconate, an accurate structure determination of lead hafnate has not previously been achieved. The problems associated with earlier structure determinations included not only those attributed to lead zirconate, namely difficulty in single crystal preparation, pseudo-symmetry, complex distortions and cell doublings, but also those arising from the even higher X-ray absorption of $PbHfO_3$. Indeed, until the recent report by Corker *et al.* (1997), describing a low-temperature (100 K) structure determination with extended scans, the details of the $PbZrO_3$ structure were still under debate. This technique was necessary in order to improve the precision of extremely weak reflections, specifically of the type h,k,l where l = odd. It was shown that previous X-ray determinations suffered from a lack of these reflections which resulted in a false manifestation of an oxygen disorder, where there were two oxygen substructures, A and B, related by the operator $x_a, y_a, z_a \rightarrow x_b, y_b, z_b + 0.5$, *i.e.* Fourier-difference maps computed with only Pb and Zr atoms in position gave two electron density peaks for each O atom. This initially resulted in the assumption that an oxygen disorder existed (Whatmore, 1976; Glazer *et al.*, 1993). Although an examination of inter-bond angles *etc.* made it a simple task to separate the possible sites into two sets which each produced geometrically reasonable oxygen octahedra, it had previously been impossible to distinguish the true oxygen subset or whether the disorder was real on the basis of the single crystal X-ray data available. This problem resulted from the pseudo-symmetry in this type of perovskite and cannot be handled by the usual least-square refinement techniques (Watkin, 1994). Although this difficulty has been known for many years, to the authors' knowledge no computing tool has been established for its treatment. Instead, the usual least-squares procedures must be utilized to determine two possible alternative solutions and then the true oxygen substructure is extracted using only a few weak l = odd reflections, which can only be obtained with adequate precision by data collection at low temperatures and with long scan times/reflection of $\frac{1}{2}$–1 h. The main conclusions of this low-temperature study of lead zirconate have now been independently confirmed by X-ray anomalous dispersion experiments (Yamasaki & Soejima, 1996).

In the following report the same procedure is used to investigate the crystal structure of the perovskite lead hafnate $PbHfO_3$ and hence determine the similarities to and differences from lead zirconate. The interest in this material arises, as with its isostructural family

Table 1. *Fractional atomic coordinates and anisotropic displacement parameters (Å²) with e.s.d.'s in parentheses, calculated from the low-temperature X-ray data collection*

$T = \exp[-2\pi^2(U^{11}h^2a^{*2} + ... 2U^{12}hka^*b^* + ...)]$.

	x	y	z	U_{iso}/U_{eq}
Pb(1)	0.6985 (2)	0.12986 (8)	0.0000	0.0025 (4)
Pb(2)	0.7146 (2)	0.1238 (1)	0.5000	0.0018 (5)
Hf(1)	0.24284 (8)	0.1237 (2)	0.2527 (8)	0.0004 (3)
O(1)	0.297 (4)	0.095 (2)	0.000	0.004 (1)
O(2)	0.272 (4)	0.150 (3)	0.500	0.004 (1)
O(3)	0.033 (3)	0.260 (1)	0.224 (2)	0.004 (1)
O(4)	0.000	0.500	0.300 (4)	0.004 (1)
O(5)	0.000	0.000	0.281 (3)	0.004 (1)

$U_{eq} = (1/3)\Sigma_i\Sigma_j U^{ij}a_i^*a_j^*\mathbf{a}_i.\mathbf{a}_j$.

	U^{11}	U^{22}	U^{33}	U^{23}	U^{13}	U^{12}
Pb(1)	0.0019 (4)	0.0051 (4)	0.0019 (4)	0.0000	0.0000	0.0012 (4)
Pb(2)	0.0041 (4)	0.0025 (4)	0.0043 (5)	0.0000	0.0000	0.0029 (5)
Hf(1)	0.0028 (2)	0.0005 (3)	0.0004 (2)	−0.0001 (3)	0.001 (1)	−0.0001 (1)

$PbZr_xTi_{1-x}O_3$, because of its possible industrial applications in the field of microelectronics and microelectromechanical systems (MEMS). Recent publications on thin films by Yamakawa *et al.* (1995) and Yamakawa *et al.* (1996) and on single crystals by Shuvaeva *et al.* (1996) reported the existence of electric-field-induced (EFI) ferroelectric phases in lead zirconate. Although investigation into the existence of these phases in lead hafnate is now in progress, an EFI phase, if found present, would also make this material an interesting candidate for charge storage applications: if a high-energy ferroelectric phase can be first induced by the application of an electric field, then at any desired time the field may be withdrawn such that the sample undergoes a phase transition into the lower energy antiferroelectric phase, simultaneously releasing polarization charge.

2. Synthesis

Lead hafnate crystals were grown from a flux using the system $PbO–B_2O_3$ as a solvent. A previous polycrystalline preparation of $PbHfO_3$ was taken in the molar proportions 0.77:0.206:0.024 ($PbO:B_2O_3:PbHfO_3$) and soaked in a platinum crucible at 1453 K for 4 h. During crystal growth, a vertical temperature gradient of 10 K cm^{-1} was maintained. The crucible was then cooled at 8 K per hour until a temperature of 1173 K was reached, at which point the solvent was poured out. The crystals were then cooled to room temperature and separated from the crucible by soaking in an aqueous solution of acetic acid. Most crystals had the form of thin, rectangular plates and had a light silver colour. Unfortunately, they also tended to be multi-domain. However, very small single-domain crystals of the size 30–40 μm, appropriate for single crystal X-ray analysis, could often be found attached to larger 0.5–1 mm multi-domain plates. These could be prized off using quartz fibres, while the large crystal plate was soaked in acetic acid under a polarizing microscope. Simple examination under a polarizing microscope could not distinguish which were suitable for single crystal X-ray analysis, as many which showed sharp extinction under the microscope were found to possess 90° twinning (such that $a \rightarrow b$ and $b \rightarrow a$) when examined carefully using X-rays. This was visible through the appearance of very weak $\frac{1}{2}kl$ reflections. Therefore, any crystals chosen for single crystal X-ray data collection were first thoroughly checked for $\frac{1}{2}kl$ reflections using extremely long scan times, typically of the order 1–2 h per reflection.

The polycrystalline samples of lead hafnate used in the neutron diffraction investigation were obtained by ball milling PbO and HfO_2 in acetone for 4 h. The resultant mixture was then allowed to dry and sieved to less than 600 microns. This was then calcined at 1423 K for 4 h in air, milled again in acetone and then sieved. The final powder was then identified as lead hafnate, indexing with cell parameters a = 5.852 (5), b = 11.716 (8) and c = 8.1997 (8) Å and checked for impurities using powder X-ray diffraction.

3. X-ray data collection

A single crystal of dimensions 0.030 × 0.030 × 0.035 mm was selected under a polarizing microscope for data collection on a Stoe Stadi-4 single crystal diffractometer using the ω–2θ scan mode and Mo $K\alpha$ radiation (λ = 0.71069 Å). At room temperature, the primitive orthorhombic cell parameters were refined using 32 reflections and least-squares methods to the values a = 5.870 (1), b = 11.758 (3) and c = 8.227 (2) Å. The crystal was then carefully checked for twinning unobserved under the polarizing microscope by thoroughly checking for $\frac{1}{2}kl$ reflections using extremely long

scans (~120 min per reflection). When no signs of twinning were observed, the crystal was cooled to 100 K using an Oxford Cryosystems Cryostream (Cosier & Glazer, 1986), at a rate of 80 K h^{-1}. The measurement of $\frac{1}{2}kl$ reflections was then repeated to check that the cooling process had not produced twinning at the contact point between the crystal and the quartz fibre on which it was mounted. The cell parameters were then redetermined and refined to the values a = 5.856 (1), 11.729 (3) and c = 8.212 (2) Å. These can be compared with a = 5.8572 (5), b = 11.689 (1) and c = 4.0971 (4) Å determined by Dernier & Remeika (1975) at 298 K, but note that in the latter work the doubling of the c axis had not been recognized because of the negligible $hk\frac{1}{2}$ reflection intensities. Single-crystal X-ray data were then collected over the 2θ range 3–68°, with $-9 < h < 9$, $-18 < k < 18$ and $-12 < l < 12$, while the scan time was increased to approximately 250 s per reflection. Three standard reflections were measured every 90 min during the data collection.

Once data collection was complete, the *hkl* reflections with l = odd were examined and 35 with the highest intensity were selected and, along with their Friedel opposites, recollected using even longer scans (approximately 2500 s per reflection). Data reduction was then performed using the program *XRED* (Stoe & Cie, 1994), giving observed systematic absences consistent with the space group *Pbam* (0*kl*: $k = 2n + 1$, *h*0*l*: $h = 2n + 1$, *h*00: $h = 2n + 1$ and 0*k*0: $k = 2n + 1$), although because of the pseudo-symmetric character of the structure, many other false sets of absences were observed, as expected. The collected data were corrected using a combination of spherical absorption (r = 15.8 μm, μr = 1.54) and ψ-scan data (T_{min} = 0.0846, T_{max} = 0.1433).

4. Data analysis and refinement procedure

The model used to initiate the refinement was based on the structure determination of lead zirconate at 100 K (Corker *et al.*, 1997). Owing to the weak intensity of important reflections, only those with $F < 1.4\sigma(F)$ were removed from the analysis before the refinement began using the program *CRYSTALS* (Watkin *et al.*, 1996), this particular cut-off value having been obtained by observing the positional parameter errors as this value was lowered. Inclusion of any weaker reflections failed to decrease errors or help correlation problems and resulted only in an artificially high R factor. The function minimized was $\Sigma\omega(|F_o| - |F_c|)^2$, where the weights were calculated using a robust/resistant weighting scheme (Prince, 1982). A separate refinement was also carried out against F_o^2, but this refinement showed no significant differences and on this occasion a better convergence was achieved when the refinement was carried out against F_o.

Refinement of parameters often converged in false minima. (Minima were assumed false if parameters were physically unreasonable or did not converge back to their original positions when shifted away.) However, by moving the fractional coordinates away from the average structure, *i.e.* by starting with a more distorted structural model than was expected, and then allowing the refinement to converge towards a more regular structure,

Table 2. *Experimental details*

Crystal data	
Chemical formula	$PbHfO_3$
Chemical formula weight	433.68
Cell setting	Orthorhombic
Space group	*Pbam*
a (Å)	5.856 (1)
b (Å)	11.729 (3)
c (Å)	8.212 (2)
V (Å^3)	564.04
Z	8
D_x (Mg m^{-3})	10.21
Radiation type	Mo $K\alpha$
Wavelength (Å)	0.71069
No. of reflections for cell parameters	20
θ range (°)	9.75–12.25
μ (mm^{-1})	97.16
Temperature (K)	100
Crystal form	Irregular
Crystal size (mm)	0.035 × 0.03 × 0.03
Crystal colour	Grey
Data collection	
Diffractometer	Stoe Stadi-4
Data Collection method	ω–2θ scans
Absorption correction	Sphere
T_{min}	0.0846
T_{max}	0.1433
No. of measured reflections	4065
No. of independent reflections	942
No. of observed reflections	439
Criterion for observed reflections	$I > 2\sigma(I)$
R_{int}	0.1046
θ_{max} (°)	34
Range of *h*,*k*,*l*	$-9 \rightarrow h \rightarrow 9$ $-18 \rightarrow k \rightarrow 18$ $-12 \rightarrow l \rightarrow 12$
No. of standard reflections	3
Frequency of standard reflections (min)	90
Intensity decay (%)	3
Refinement	
Refinement on	F
R	0.0383
wR	0.0447
S	1.07
No. of reflections used in refinement	439
No. of parameters used	33
Weighting scheme	Tukey and Prince (Prince, 1982), three parameters: 19.9, −20.1, 15.0
$(\Delta/\sigma)_{max}$	0.0001
$\Delta\rho_{max}$ (e Å^{-3})	3.4
$\Delta\rho_{min}$ (e Å^{-3})	−4.1
Extinction method	Larson (1970)
Extinction coefficient	8.7 (6)
Source of atomic scattering factors	*International Tables for X-ray Crystallography* (1974, Vol. IV)

Table 3. *R factors for different models separated into layers of different l*

Layer	No. of data	True ordered model substructure *B*		False ordered model substructure *A*		Disorder model 50% *A* and 50% *B*	
		R	*wR*	*R*	*wR*	*R*	*wR*
$l = 1$	9	0.2508	0.1063	0.5906	0.5390	0.4210	0.3062
$l = 3$	6	0.0639	0.0513	0.4605	0.4631	0.2317	0.2315
$l = 5$	7	0.1258	0.1113	0.5371	0.4493	0.3741	0.3168
$l = 7$	4	0.0378	0.0586	0.3884	0.3700	0.2097	0.2005
$l = 0$	88	0.0413	0.0458	0.0409	0.0458	0.0410	0.0458
$l = 2$	87	0.0316	0.0408	0.0315	0.0406	0.0315	0.0406
$l = 4$	81	0.0362	0.0429	0.0367	0.0432	0.0367	0.0432
$l = 6$	65	0.0373	0.0465	0.0373	0.0467	0.0373	0.0467
$l = 8$	54	0.0346	0.0440	0.0344	0.0440	0.0345	0.0440
$l = 10$	29	0.0368	0.0442	0.0367	0.0438	0.0366	0.0438
$l = 12$	9	0.0328	0.0334	0.0337	0.0343	0.0335	0.0341
		Total $R = 0.0383$ $wR = 0.0447$		Total $R = 0.0450$ $wR = 0.0692$		Total $R = 0.0417$ $wR = 0.0536$	

rather than starting with a more regular structure and attempting to refine to the true distorted structure, it was possible to avoid false minima. High correlation did, however, continue, especially between the two sets of independent Pb thermal parameters, preventing a convergence to physically reasonable values. Hence, those given in Table 1 were obtained by refining the thermal parameters of Pb(1) and Pb(2) separately. The only other correlation problem that did not disappear when weak reflections were included, in comparison to using a more conventional $F < 3\sigma(F)$ cut-off, was a high correlation between the displacement parameter U^{33} and the z parameter of Hf(1). If refined together an unreasonably high displacement factor would be accompanied by large oscillations of the Hf atoms above and below the $z = 0.25$ plane. However, by again alternatively refining the hafnium positional and displacement parameters and also by initially including large damping coefficients, a sensible convergence was reached. The final positional and displacement parameters are given in Table 1, while a summary of experimental details are given in Table 2.†

As a check on the true positional parameters of the oxygens, the *R* factor was analysed in terms of its contributions from odd and even '*l*' layers. This was carried out not only on the final ordered oxygen model (named here substructure *B*), but also with its 'opposite' substructure (where $x_a, y_a, z_a \rightarrow x_b, y_b, z_b + 0.5$) and with a disordered oxygen model (50% *A* and 50% *B*). The contributions in each case are summarized in Table 3. Clearly, although the high-intensity l = even reflections are unable to distinguish between the three models, there are considerable differences in the l = odd contributions. Owing to their very weak intensities, contributions to the *R* factor are unfortunately high in all cases. However, their fit is sufficient to distinguish the true structure.

† A list of structure factors and the numbered intensity of each measured point on the profile have been deposited with the IUCr (Reference: NA0080). Copies may be obtained through The Managing Editor, International Union of Crystallography, 5 Abbey Square, Chester CH1 2HU, England.

5. Birefringence measurements

Low-temperature X-ray data collections are extremely beneficial for the examination of the room-temperature crystal structures of both lead hafnate and lead zirconate. However, to date, it has only been *assumed* that no phase transition exists between 100 K and room temperature. Indeed, although the oxygen disorder previously reported has now been shown to be simply a manifestation resulting from an inadequate number of l = odd reflections with significant intensity, this has only been shown at 100 K. It is hence possible to argue that without an investigation into low-temperature phase transitions, a disorder, although now unlikely, may still be present at room temperature which is where the overall interest in these structures lies. It was therefore decided to investigate the possibility of further unknown phase transitions by making continuous birefringence measurements whilst varying the temperature for both lead zirconate and lead hafnate.

The rotating analyser technique was used for this experiment. Described by Wood & Glazer (1980), this technique is both highly sensitive and convenient for making continuous measurements needed to identify a phase transition.

Platelet crystals of $PbZrO_3$ and $PbHfO_3$ with dimensions 1.4 × 1.5 × 0.1 mm and 0.9 × 0.3 × 0.04 mm, respectively, were selected under a polarizing microscope. Unfortunately, neither of these crystals were single domain and hence the actual retardation measurements are not absolute birefringence measurements. However, as the domain structure in both crystals remained constant throughout the experiment, the retardation observed was still sensitive to the kind of optical change expected at a phase transition. By this technique the change in retardation was monitored continuously over the temperature ranges 97–298 and 77–298 K, respectively. Apart from a small continuous decrease in retardation as the temperature was allowed to increase, no anomalies indicative of a phase transition were observed. The absence of an additional low-temperature

phase transition is now also supported by the recent work by Miga (1996), in which S-domain wall orientation was investigated with temperature.

6. Neutron data collection and Rietveld analysis

A neutron powder pattern of lead hafnate was collected on diffractometer D1A at the Institut Max von Laue–Paul Langevin. Data were collected using λ = 1.90788 Å at 383 K. Although a neutron data collection at 100 K would have given the possibility of achieving a better determination of the structure as a refinement of combined X-ray and neutron data may have been attempted, a high-temperature collection was performed. This was partially due to practicalities at the time, but primarily so that the results would be comparable with the neutron refinement previously published by Corker *et al.* (1997). Lead hafnate undergoes a phase transition at around 393 K and hence it was decided that a collection at 383 K was sufficiently far from the transition and yet would still hold useful information for comparison with lead zirconate (previously reported at 398 K).

Data were collected to θ_{max} = 79.48°, $\Delta\theta$ = 0.025° with the sample held in a vanadium cylindrical holder (1 cm diameter, 6 cm height). Owing to the high cross section of hafnium an absorption factor was applied to the data and then a Rietveld refinement performed using the program *FULLPROF* (Rodriguez-Carvajal, 1995). Neutron elastic scattering lengths b_{Pb} = 9.405, b_{Hf} = 7.800 and b_O = 5.803 fm were used, while the background was refined using a polynomial function. Several types of peak profiles were investigated, but the best fit was obtained with the peak shape described by a pseudo-Voigt function.

The initial model used in the refinement was based on that obtained from the low-temperature X-ray refinement. As this would be expected to be an even more distorted structure this prevented a false convergence to a more average structure. However, as we know from experience that many false convergences can easily occur in these highly pseudo-symmetric structures, the refinement model was repeatedly altered in order to check that the final coordinates obtained were consistent within the errors given. Pb and Hf atoms were refined anisotropically, but because of the high parameter-to-reflection ratio all oxygens were kept isotropic. This problem was compounded by the need to exclude several regions of the neutron pattern from the refinement owing to extra peaks arising from the furnace surrounding the sample. The highest of these impurity peaks is at 2θ = 48.70°, which can be seen in Fig. 1, where the calculated, observed and difference profiles of lead hafnate are shown.

Final positional and thermal parameters are given in Table 4 while associated experimental details are given in Table 5.

7. Results and discussion

Originating from the simple cubic structure at high temperature, the room-temperature phase of lead hafnate can most easily be described by its relative cation shifts and octahedral tilts and distortions from this average

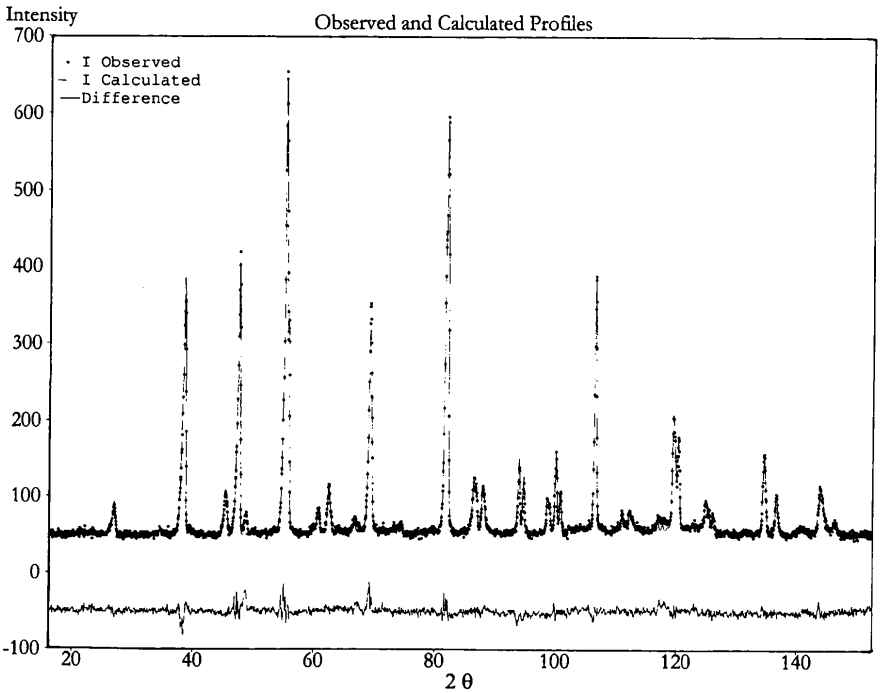

Fig. 1. Observed and calculated neutron diffraction patterns.

Table 4. *Fractional atomic coordinates and anisotropic displacement parameters ($Å^2$) with e.s.d.'s in parentheses, calculated from the neutron Rietveld refinement of $PbHfO_3$ at 383 K*

$T = \exp[-2\pi^2(U^{11}h^2a^{*2} + ...2U^{12}hka^*b^* + ...)]$.

	x	y	z	U_{iso}/U_{eq}
Pb(1)	0.734 (2)	0.1278 (8)	0.0000	0.044 (5)
Pb(2)	0.723 (2)	0.1252 (9)	0.5000	0.034 (6)
Hf(1)	0.2464 (9)	0.1272 (7)	0.2493 (9)	0.004 (3)
O(1)	0.275 (3)	0.093 (1)	0.000	0.027 (3)
O(2)	0.273 (2)	0.1439 (9)	0.500	0.015 (3)
O(3)	0.021 (2)	0.2562 (8)	0.220 (1)	0.041 (3)
O(4)	0.000	0.500	0.270 (1)	0.017 (2)
O(5)	0.000	0.000	0.276 (1)	0.015 (2)

$U_{eq} = (1/3)\Sigma_i\Sigma_j U^{ij}a_i^*a_j^*\mathbf{a}_i.\mathbf{a}_j$.

	U^{11}	U^{22}	U^{33}	U^{23}	U^{13}	U^{12}
Pb(1)	0.077 (5)	0.024 (3)	0.048 (3)	0.0000	0.0000	−0.011 (5)
Pb(2)	0.037 (4)	0.058 (3)	0.019 (2)	0.0000	0.0000	−0.003(6)
Hf(1)	0.022 (2)	0.004 (2)	0.010 (1)	−0.002 (1)	0.012 (3)	0.002 (2)

Table 5. *Experimental details*

Crystal data	
Chemical formula	$PbHfO_3$
Chemical formula weight	433.68
Cell system	Orthorhombic
Space group	*Pbam*
a (Å)	5.8582 (3)
b (Å)	11.7224 (5)
c (Å)	8.2246 (3)
V ($Å^3$)	564.80
Z	8
D_x ($Mg\ m^{-3}$)	10.20
Radiation type	Neutron
Wavelength (Å)	1.90788
θ range (°)	0.0–79.475
Temperature (K)	383
Data collection	
Diffractometer	D1A, ILL
Monochromator	Germanium
Sample container	Vanadium holder
Instrument geometry	25 ^{3}He detectors
2θ step (°)	0.05
θ_{max} (°)	79.475
Refinement	
Background	Polynomial function
R (least-squares)	0.0463
R (Rietveld)	0.167
wR (least-squares)	0.0587
wR (Rietveld)	0.141
R_{exp} (least-squares)	0.0461
R_{exp} (Rietveld)	0.1110
χ^2	0.0162
No. of parameters used	52
Full width at half-maximum	$u\tan^2\theta + v\tan\theta + w$
Weighting scheme	$w = (\sigma^2)^{-1}$
Analytic function for profile	Pseudo-Voigt
$(\Delta/\sigma)_{max}$	0.1
$R_I = \Sigma(Ii - Ici)/\Sigma Ii$	0.074
Computer programs	
Refinement	*Fullprof* (Rodriguez-Carvajal, 1995)
Graphics	*Crystallographica* (Oxford Cryosystems, 1996)

structure. Throughout this discussion lead zirconate, the end member of the technological important series PZT, is also compared.

Originally the Pb atoms are 12-fold coordinated by oxygens in their high-temperature cubic phase. However, as the temperature is lowered to room temperature, the displacements which occur give rize to a highly asymmetric Pb—O bond arrangement. With four bonds considerably shortened, the Pb atoms sit at the apex of a pyramid. This arrangement is displayed for Pb(1) and Pb(2) sites in Figs. 2(*a*) and 2(*b*), respectively, while Pb—O bond distances are reported in Table 6.

When examining the Pb displacements from their original cubic positions it is initially important to separate the displacements into [100] and [010] shifts. These are listed for $PbHfO_3$ and $PbZrO_3$ in Table 7. Examining these shifts independently reveals several different features consistent for both lead hafnate and lead zirconate. Firstly, the major shift undergone by Pb is the [100] shift. Indeed, at 100 K this displacement is an order of magnitude greater than that along [010]. However, this difference does diminish as the temperature increases and sites gradually move to their high-temperature high-symmetry positions. Secondly, the Pb(1) position in these compounds behaves quite differently from the Pb(2) site as the temperature is changed. While the Pb(1) [100] shift seems dominant in both the low-temperature refinements, it is this shift, rather than that of Pb(2), which quickly diminishes as the temperature is increased. In lead hafnate, while the Pb(1) shift diminishes by around 75% between the 100 and 383 K determinations, the Pb(2) shift only drops by 20%. This is mirrored in lead zirconate, where the Pb(2) shift displays virtually no change between the low-temperature X-ray and high-temperature neutron refinement.

The Pb(1) coordination also shows considerably more distortion than that of Pb(2) with three of its four bonds much shorter, such that Pb(1) could be regarded as

threefold coordinated. Looking at the low-temperature refinements of both $PbZrO_3$ and $PbHfO_3$, as it is in these cases where the distortion is more pronounced, there is an extremely strong similarity in the way Pb(1) and Pb(2) behave in both compounds. For instance, considering the fourfold coordination, the average Pb(1)—O distance is 2.47 Å in $PbHfO_3$ and 2.48 Å in $PbZrO_3$, and again in both cases there is an almost identical increase in the average Pb(2)—O distance, to 2.58 and 2.56 Å for $PbHfO_3$ and PbZrO, respectively. There is also a high similarity between the fifth shortest bond lengths. For Pb(2) these are 2.85 Å for both materials and for Pb(1) 3.09 and 3.11 Å for lead hafnate and lead zirconate, respectively. The relative increase in the fifth bond distance for Pb(1) again shows the more pronounced distorted environment in comparison with the Pb(2) site.

Considering the bonding to either three or four oxygens it would seem that Pb^{2+} forms bonds which are highly covalent. Indeed, the bonding has many similarities, in the type of distortion and bond lengths observed, to that of lead tetraborate, where non-centrosymmetric Pb—O bonding is responsible for the material's high optical non-linearity (Corker & Glazer, 1996). Although in $PbHfO_3$ and $PbZrO_3$ the structures

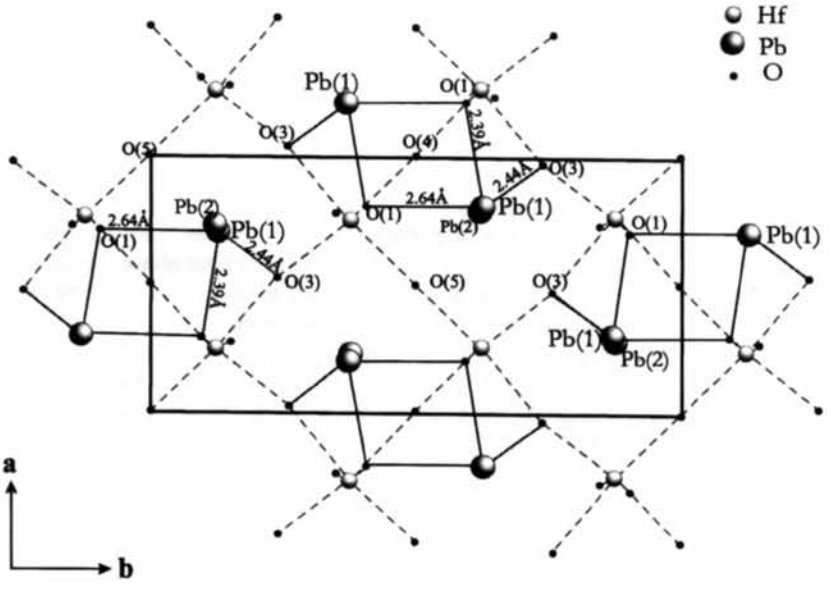

(*a*)

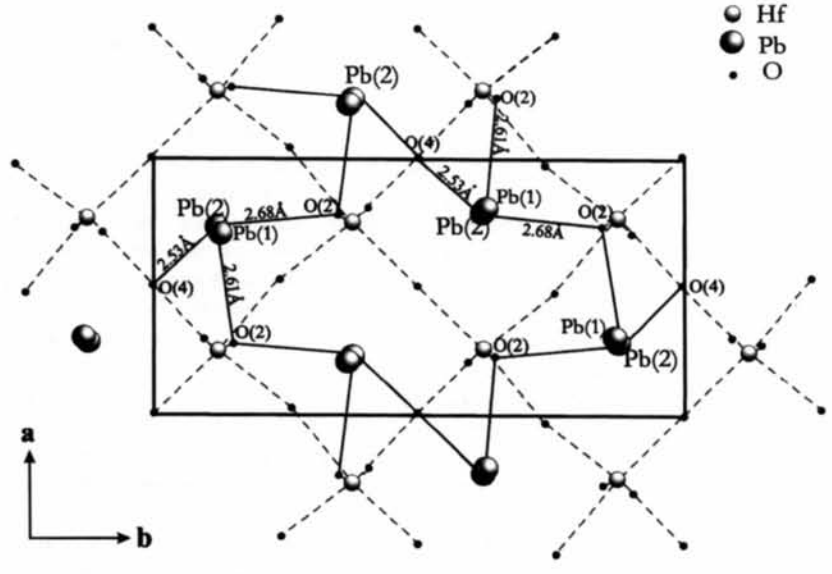

(*b*)

Fig. 2. (*a*) Pb(1)—O and (*b*) Pb(2)—O bonding in the HfO_6 network.

Table 6. *Pb—O bond lengths (Å) for lead hafnate at 100 and 383 K*

Lead zirconate distances included for comparison taken from Corker *et al.* (1997).

$PbHfO_3$ 100 K		$PbHfO_3$ 383 K†	
Pb(1)—O(3)	2.44 (2) ×2	Pb(1)—O(3)	2.59 (1) ×2
Pb(1)—O(1)	2.39 (3)	Pb(1)—O(1)	2.59 (1)
Pb(1)—O(1)	2.64 (2)	Pb(1)—O(1)	2.72 (1)
Pb(1)—O(3)	3.09 (1) ×2	Pb(1)—O(3)	2.89 (1) ×2
Pb(2)—O(4)	2.53 (2) ×2	Pb(2)—O(4)	2.73 (1) ×2
Pb(2)—O(2)	2.61 (2)	Pb(2)—O(2)	2.65 (1)
Pb(2)—O(2)	2.68 (3)	Pb(2)—O(2)	2.72 (1)
Pb(2)—O(3)	2.85 (1) ×2	Pb(2)—O(5)	2.86 (1) ×2
$PbZrO_3$ 100 K		$PbZrO_3$ 398 K	
Pb(1)—O(3)	2.42 (1)	Pb(1)—O(3)	2.538 (7)
Pb(1)—O(1)	2.41 (1)	Pb(1)—O(1)	2.53 (1)
Pb(1)—O(1)	2.67 (1)	Pb(1)—O(1)	2.71 (1)
Pb(1)—O(3)	3.105 (9)	Pb(1)—O(3)	3.016 (7)
Pb(2)—O(4)	2.529 (9)	Pb(2)—O(4)	2.580 (6)
Pb(2)—O(2)	2.55 (1)	Pb(2)—O(2)	2.58 (1)
Pb(2)—O(2)	2.64 (1)	Pb(2)—O(2)	2.64 (1)
Pb(2)—O(3)	2.851 (9)	Pb(2)—O(3)	2.831 (7)

† Errors for high-temperature neutron refinements of both lead hafnate and zirconate were calculated using Cruickshank's relation (Carpenter, 1979).

Table 7. *Cation antiparallel shifts from cubic positions*

$PbHfO_3$	$PbZrO_3$
Pb(1) [100] shift 0.30 Å (100 K)	Pb(1) [100] shift 0.30 Å (100 K)
Pb(2) [100] shift 0.21 Å (100 K)	Pb(2) [100] shift 0.26 Å (100 K)
Pb(1) [100] shift 0.08 Å (383 K)	Pb(1) [100] shift 0.19 Å (398 K)
Pb(2) [100] shift 0.17 Å (383 K)	Pb(2) [100] shift 0.25 Å (398 K)
Pb(1) [010] shift 0.06 Å (100 K)	Pb(1) [010] shift 0.06 Å (100 K)
Pb(2) [010] shift 0.01 Å (100 K)	Pb(2) [010] shift 0.02 Å (100 K)
Pb(1) [010] shift 0.03 Å (383 K)	Pb(1) [010] shift 0.07 Å (398 K)
Pb(2) [010] shift 0.00 Å (383 K)	Pb(2) [010] shift 0.02 Å (398 K)
Hf(1) [001] shift 0.022 Å (100 K)	Zr(1) [001] shift 0.008 Å (100 K)

are centrosymmetric and hence cannot show optical non-linearity as in lead tetraborate, this similarity signifies the high degree of covalency of this type of Pb—O asymmetric bonding. If this type of bonding is favoured by Pb as temperature is reduced and can most easily be accommodated by Pb displacements and ZrO_6 octahedral tilting (rather than by a phase transition into a completely different structure), then it seems likely that it is the Pb atoms that play a significant role in forming the type of pseudo-symmetric structure we have observed in $PbZrO_3$ and $PbHfO_3$, *i.e.* the type of octahedral tilting and deformation seen is such as to accommodate the nature of the Pb—O bonding rather than *vice versa*.

The final point to be noticed about the cation shifts is that of the Hf (or Zr). These not only exhibit the [100] and [010] shifts experienced by the Pb atoms but, more interestingly, they also experience anti-parallel [001] shifts. This point was initially noticed after the low-temperature structure analysis of lead zirconate. However, in $PbZrO_3$ the [001] displacement was found to be very small (0.008 Å) and with no other publications of this shift to compare with, this result had to viewed with caution. Indeed, the [001] displacement is so small that within experimental errors it cannot be seen at all in the high-temperature neutron studies of both materials. However, the single crystal low-temperature study of lead hafnate shows this type of shift to be much larger (0.022 Å) and hence more reliably determined, thus providing evidence that it is a real effect in $PbZrO_3$ also.

Another consequence of this structure determination of lead hafnate, especially of the cation shifts, is the certainty of the space-group assignment. For many years there has been much argument over whether the true space group of lead zirconate is *Pbam* or *Pba*2 and hence if the material is centrosymmetric or non-centrosymmetric. Indeed, for several years many techniques have been used and physical properties repeatedly measured to make this distinction, including piezoelectricity and ferroelectricity by Dai *et al.* (1995), Roberts (1951), energetic calculations by Singh (1995) and convergent-beam electron diffraction by Tanaka *et al.* (1982). However, if we are to assume that the two materials are isostructural and have the same space group, which seems logical considering the close similarity observed between the structural details, then the very distinct anti-parallel [001] shift of the hafnium and the comparatively small displacement parameters obtained further supports the space-group assignment of *Pbam*. If the true space group were *Pba*2, then parallel [001] shifts of both Pb and Hf could be present, rather than being constrained to be anti-parallel as observed for Hf with the space group *Pbam*. Refinement of the cation positions in space group *Pba*2 showed no such parallel [001] shifts within experimental errors, although clearly the accuracy of the refinement was reduced because of the increase in the number of variable parameters. Furthermore, if the space group were really *Pba*2, then two independent Hf general positions would be replaced by one when the structure is refined in *Pbam*. The averaging of the positional parameters that this would enforce would likely lead not only to large errors, but also to large displacement parameters. In the low-temperature refinements of both lead zirconate and hafnate, where the accuracy of the cations is greatest, the displacement parameters are clearly observed to be small. (The same displacement parameters determined in space group *Pba*2 were, if anything, larger.)

Details of the Hf and Zr octahedral environment are shown in Figs. 3 and 4, in which the $PbHfO_3$ structure (at 100 K) is viewed down the *c* and *a* axes, respectively. Associated bond lengths and angles are again given for both $PbHfO_3$ and $PbZrO_3$ at high and low temperatures for comparison in Tables 8 and 9. The deviation from the octahedral structure in the high-temperature cubic phase can be seen by examining the octahedral tilting and

distortion. The combination of octahedral tilting and hafnium displacements is shown by the Hf—O—Hf bonds, while the extent of octahedral distortion alone can be seen from the angle made at the hafnium, *i.e.* O—Hf—O and the associated bond lengths. The mean Hf—O and Zr—O bonds lengths in all four refinements are seen to be almost identical with only a slight increase for the Zr—O bonds as one may expect (ionic radii Zr:

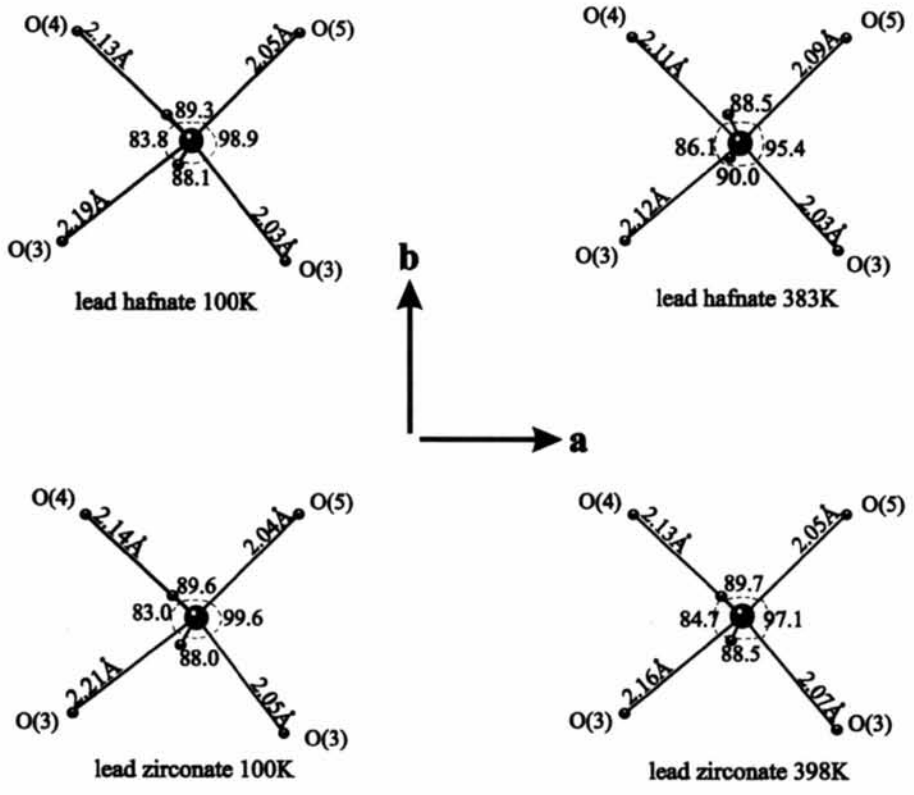

Fig. 3. Octahedral viewed down the *c* axis showing the change in Zr/Hf—O bonding with increase in temperature.

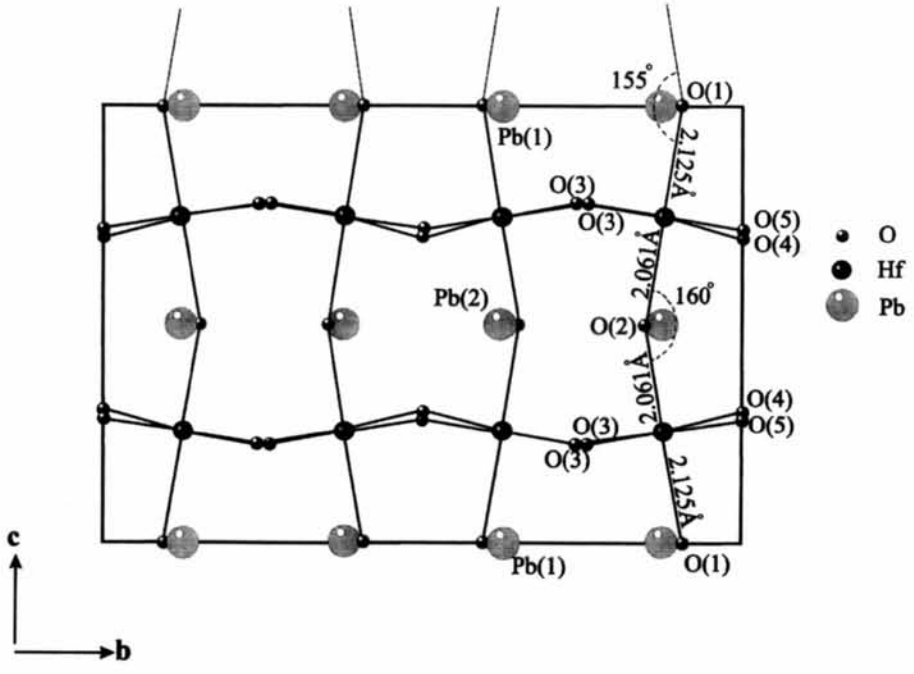

Fig. 4. HfO_6 tilts viewed down the *a* axis.

Table 8. *Bond lengths (Å) for the HfO_6/ZrO_6 octahedra*

$PbHfO_3$ 100K		$PbHfO_3$ 383 K†	
Hf(1)—O(1)	2.125 (9)	Hf(1)—O(1)	2.10 (1)
Hf(1)—O(2)	2.061 (8)	Hf(1)—O(2)	2.08 (1)
Hf(1)—O(3)	2.03 (1)	Hf(1)—O(3)	2.02 (1)
Hf(1)—O(3)	2.19 (1)	Hf(1)—O(3)	2.12 (1)
Hf(1)—O(4)	2.127 (6)	Hf(1)—O(4)	2.112 (9)
Hf(1)—O(5)	2.045 (3)	Hf(1)—O(5)	2.087 (9)
$PbZrO_3$ 100 K		$PbZrO_3$ 398 K	
Zr(1)—O(1)	2.098 (5)	Zr(1)—O(1)	2.11 (1)
Zr(1)—O(2)	2.111 (5)	Zr(1)—O(2)	2.09 (1)
Zr(1)—O(3)	2.047 (8)	Zr(1)—O(3)	2.067 (8)
Zr(2)—O(3)	2.205 (8)	Zr(2)—O(3)	2.162 (8)
Zr(2)—O(4)	2.142 (3)	Zr(2)—O(4)	2.125 (7)
Zr(2)—O(5)	2.044 (2)	Zr(2)—O(5)	2.053 (8)

† Errors for high-temperature neutron refinements of both lead hafnate and zirconate were calculated using Cruickshank's relation (Carpenter, 1979).

Table 9. *Bond angles (°) for the HfO_6/ZrO_6 octahedra*

$PbHfO_3$ 100 K		$PbHfO_3$ 383 K†	
Hf(1)—O(1)—Hf(1)	155 (1)	Hf(1)—O(1)—Hf(1)	156.2 (4)
Hf(1)—O(2)—Hf(1)	160 (2)	Hf(1)—O(2)—Hf(1)	166.2 (4)
Hf(1)—O(3)—Hf(1)	160.9 (9)	Hf(1)—O(3)—Hf(1)	164.3 (4)
Hf(1)—O(4)—Hf(1)	159 (2)	Hf(1)—O(4)—Hf(1)	170.9 (3)
Hf(1)—O(5)—Hf(1)	167 (1)	Hf(1)—O(5)—Hf(1)	167.8 (3)
$PbZrO_3$ 100 K		$PbZrO_3$ 398 K	
Zr(1)—O(1)—Zr(1)	155.3 (7)	Zr(1)—O(1)—Zr(1)	157.7 (4)
Zr(1)—O(2)—Zr(1)	156.4 (7)	Zr(1)—O(2)—Zr(1)	159.7 (4)
Zr(1)—O(3)—Zr(1)	160.0 (5)	Zr(1)—O(3)—Zr(1)	164.2 (3)
Zr(1)—O(4)—Zr(1)	158.9 (8)	Zr(1)—O(4)—Zr(1)	161.4 (3)
Zr(1)—O(5)—Zr(1)	170.2 (8)	Zr(1)—O(5)—Zr(1)	169.8 (3)

† Errors for high-temperature neutron refinements of both lead hafnate and zirconate were calculated using Cruickshank's relation (Carpenter, 1979).

0.79 Å, Hf: 0.78 Å). However, as the temperature decreases the deviation from this average bond length shows a significant increase of around 50% for both materials, resulting in the pattern of long and short bonds shown in Fig. 3, where the four bonds approximately lying in the *ab* plane are observed. The four angles made by these bonds at the Hf consist of two which remain at around 90°, and one larger and one smaller angle, with only the latter two showing significantly greater deviation as the temperature falls. The largest angle is formed between the two shortest bonds and the smallest angle between the two longest, while the 90° angles are formed between one short and one long bond. Because O(4) and O(5) are locked in special positions, the octahedra are highly distorted in the (001) projection, so that one cannot really describe any form of octahedral tilting about the *c* axis. However, on looking along the pseudocubic a_p and b_p axes, antiphase tilting is observed so that the nearest tilt system notation (Glazer, 1972) that can be applied is $a^-a^-c^0$.

In Fig. 4 the remaining two Hf(Zr)—O bonds showing a similar short and long configuration around the central Hf (Zr) atom are seen. (Details in Fig. 4 are those associated with the 100 K $PbHfO_3$ refinement.) This figure also shows more clearly the octahedral tilting observed. In an untilted, regular octahedral network the Hf—O—Hf (or Zr—O—Zr) angles would become 180° but, as can be seen from Table 9, the deviations from this value are quite considerable, increasing to an average of 20° for the low-temperature structures of both materials. At each temperature and in both compounds the largest variation, approximately 25° for the 100 K structures, is that associated with O(1). This factor is probably associated with the more highly distorted O environment of Pb(1), with Pb(1)—O(1) being the shortest Pb—O bond.

In conclusion, the present X-ray and neutron investigations have not only allowed the crystal structure details of lead hafnate to be calculated, but also due to their similar characteristics, has given further insight into the character and behaviour of the more well known material lead zirconate.

The authors would like to thank the Institut Max von Laue–Paul Langevin (ILL), Grenoble, France, for allowing the neutron diffraction experiment to be carried out. We would also like to thank Dr Francois Fauth for his assistance during our time at the ILL and for his continuing support. We would also like to express gratitude to the Engineering and Physical Sciences Research Council (EPSRC) for providing the grant for this investigation. One of the authors, K. Roleder, is grateful to the Oxford Colleges Hospitality Scheme and the Stefan Batory Trust for grants to enable this work to be carried out.

References

Carpenter, G. B. (1979). *Acta Cryst.* A**37**, 248–250.
Corker, D. L. & Glazer, A. M. (1996). *Acta Cryst.* B**52**, 260–265.
Corker, D. L., Glazer, A. M., Dec, J., Roleder, K. & Whatmore, R. (1997). *Acta Cryst.* B**53**, 135–142.
Cosier, J. & Glazer, A. M. (1986). *J. Appl. Cryst.* **19**, 105–107.
Dai, X., Li, J. F. & Viehland, D. (1995). *Phys. Rev. B*, **51**, 2651–2655.
Dernier, P. D. & Remeika, J. P. (1975). *Mat. Res. Bull.* **10**, 187–192.
Glazer, A. M. (1972). *Acta Cryst.* B**28**, 3384–3392.
Glazer, A. M., Roleder, K. & Dec, J. (1993). *Acta Cryst.* B**49**, 846–852.
Larson, A. C. (1970). *Crystallographic Computing*, edited by F. R. Ahmed, pp. 291–294. Munksgaard: Copenhagen.
Leont'ev, N. G., Kolesova, R. V., Eremkin, V. V., Fesenko, O. E. & Smotrakov, V. G. (1984). *Sov. Phys. Crystallogr.* **29**, 238–239.
Oxford Cryosystems (1996). *Crystallographica. A Crystallographic Data Software Tool.* Oxford Cryosystems, Long Hanborough, England.
Miga, S. (1996). Ph.D. Thesis. University of Silesia, Poland.

Prince, E. (1982). *Mathematical Techniques in Crystallography and Materials Science*. Berlin: Springer-Verlag.
Roberts, S. (1951). *Phys. Rev.* **83**, 1078.
Rodriguez-Carvajal, J. (1995). *FULLPROF. A Rietveld Refinement and Pattern Matching Analysis Program*. Laboratoire Leon Brillouin (CEA-CNRS), France.
Shirane, G. & Pepinsky, J. P. (1953). *Phys. Rev.* **91**, 812–815.
Shuvaeva, V. A., Antipin, M. Yu., Fesenko, O. E. & Struchkov, Yu. T. (1996). *J. Phys. Condens. Matter*, **8**, 1615–1620.
Singh, D. J. (1995). *Phys. Rev. B*, **52**, 12559–12563.
Stoe & Cie (1994). *X-RED Data Reduction Program, STADI4 Data Collection Program*. Stoe & Cie, Darmstadt, Germany.
Tanaka, M., Saito, R. & Tsuzuki, K. (1982). *J. Phys. Soc. Jpn*, **51**, 2635–2640.
Watkin, D. J. (1994). *Acta Cryst.* A**50**, 411–437.
Watkin, D. J., Prout, C. K., Carruthers, J. R. & Betteridge, P. W. (1996). *CRYSTALS*. Issue 10. Chemical Crystallography Laboratory, The University of Oxford.
Whatmore, R. W. (1976). D.Phil. Thesis. Cavendish Laboratory, Cambridge, England.
Wood, I. G. & Glazer, A. M. (1980). *J. Appl. Cryst.* **13**, 217–223.
Yamakawa, K., Gachigi, K. W. A., Trolier-McKinstry S. & Dougherty, J. P. (1996). *Ferroelectr. Lett.* **20**, 149–155.
Yamakawa, K., Trolier-McKinstry, S., Dougherty, J. P. & Krupanidhi, S. B. (1995). *Appl. Phys. Lett.* **67**, 2014–2016.
Yamasaki, K. & Soejima, Y. (1996). *Acta Cryst.* A**52**, C-47.
Zaitsev, S. M., Zhavoronko, G. P., Tatarenko, A. A., Kupryanov, M. F., Filip'ev, V. S. & Fesenko, E. G. (1979). *Sov. Phys. Crystallogr.* **24**, 474–475.